Wound healing and skin regeneration on FT-skin

Marisa Meloni[1], Bernadette Lombardi[2], Francesco Carriero[1], Laura Ceriotti[1]*

[1]VitroScreen Srl, Milan, Italy; [2]Telethon Institute of Genetics and Medicine (TIGEM), Pozzuoli, Italy.

Laura Ceriotti, VitroScreen Srl, via Mosè Bianchi 103, 0039-02-89077608,
laura.ceriotti@vitroscreen.com

Abstract

Background: Skin regeneration is a physiological but complex process involving the reorganization of different cell types to restore tissue continuity after injury. The aim of this research project was to develop an *in vitro* experimental model on 3D reconstructed Full Thickness (FT) skin that in a relatively short experimental window was able to recapitulate fibroblasts activation and ECM remodeling.

Methods: A FT-Skin model was injured with 1-mm biopsy punch. The wound bed evolution was followed by a time course approach: 24h and 3-8 days. Immuno-histochemical analysis (α-SMA, fibronectin) was applied to qualitatively and quantitatively capture cell migration, polarization and differentiation and ECM remodeling.

Results: The migration of keratinocytes was confirmed by analyzing CK14 and ITG β1 expression and localization in the wound bed. The role of activated fibroblasts-myofibroblasts as major players in the ECM remodeling process has been demonstrated by a-smooth muscle actin and fibronectin localization by immunofluorescence analysis: a fully restored skin integrity was observed at day 8.

Conclusion: We have demonstrated that by using standardized injury procedure an *in vitro* reconstructed 3D FT-skin was able to recapitulate the main steps of the skin regeneration and healing process in the two skin compartments with results in good agreement with literature data and clinical findings. The approach described seems promising to assess dermo-pharmaceutical and cosmetic formulations efficacy.

Keywords: Wounds; Skin regeneration; α-SMA; fibronectin; FT-skin model

Introduction.

Several *in vitro* preclinical models on 3D skin analogs able to recapitulate single mechanisms activated during repair process as gap closure, re-epithelialization, connective tissue repair and scarring have been described in literature [1-5]. The aim of this research work was to develop an *in vitro* experimental model on a commercial available 3D Full Thickness skin model able to recapitulate skin regeneration dynamic over time highlighting the cell machineries involved.

Materials and Methods.

Test system

Phenion® Full Thickness Skin Model (FT-Skin-standard diameter 1.4 cm) is a commercially available model produced by Henkel (Düsseldorf, Germany) [6-8]. Epidermal keratinocytes and dermal fibroblasts (derived from the same healthy human donor) are used to form a multilayered skin equivalent that resembles human skin under culture conditions. Keratinocytes are first overlaid on an artificial dermis and then grown in air-liquid interface until developing of an epidermis with clearly recognizable layers. The dermal compartment is composed of fibroblasts embedded in an exogenous proprietary scaffold that does not contract under cell traction forces. The epidermis has been characterized by the expression of differentiation markers. The epidermal-dermal junction presents basal membrane proteins (Laminin and Collagen IV) Papillary dermis is highly populated by fibroblasts and de novo synthesis of ECM has been demonstrated in terms of elastin and fibronectin. After reception the tissues were removed from the semi-solid transport medium and cultivated at 37°C and 5% CO_2 with ALI® Culture Medium according to the supplier's instructions.

Experimental design

The FT-skin series codes corresponding to different experimental conditions are presented in Table 1. The FT-skin tissues were injured at both epidermal and dermal level as described in Figure 1. At define time-points, FT-skin models were collected, and tissue were fixed in 10% buffered formalin for histological and immuno-histological analysis (day 1 to day 8 days). All experiments were conducted on biological triplicates. Three independent experiments for WM and AWM were performed.

Table 1. Codes. Series codes where Day_ indicates the culture time after injury.

FT-skin series: CODES	**DESCRIPTION**
DAY_ NC	FT- skin Negative Control not injured and cultured overtime
DAY_ WM	Injured FT-skin cultured overtime with ALI medium
DAY_ AWM	Injured FT-skin cultured overtime with 2-O-α-D-Glucopyranosyl-L-Ascorbic Acid (L-AA) (Merk Life Science, cod. SMB00390) 15>mg/mL<75 in ALI medium

Injury procedure

A sterile 1-mm biopsy punch with plunger was used to induce a physical discontinuity in both epidermis and dermis in the FT-Skin. With a sterile pair of tweezers, the FT-Skin were transferred in a Petri dish and injured with the punch biopsy in two different parts of the tissue symmetrically (panel A_2). The 1-mm biopsy punch cut, perforate and remove a small and defined piece of tissue to create the physical discontinuity in both epidermis and dermis layers (Figure 1).

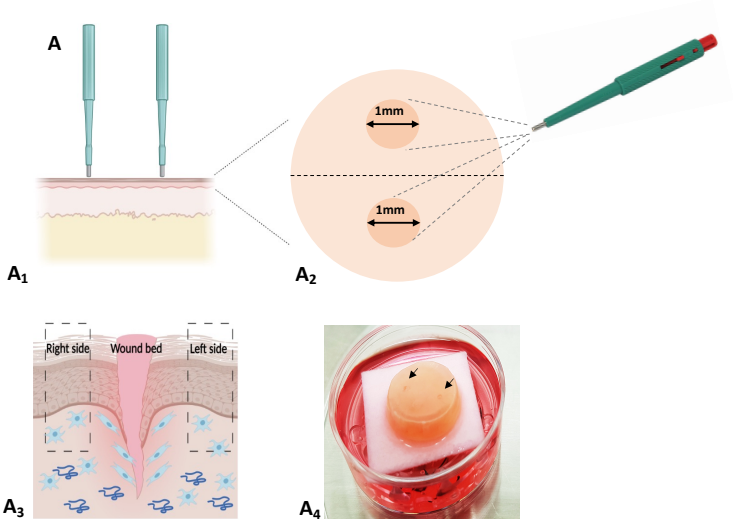

Figure 1. Injury procedure. A) Schematic representation of injury procedure in a FT-Skin model: each FT-Skin is wounded with a 1-mm biopsy punch with plugger. A1) Cross section during injury procedure. A2) Skin surface sketch after injury; two injuries are performed with respect to the symmetry axis of the tissue. A3) Design of the wounded FT-Skin: injury creates a physical discontinuity in both epidermis and dermis layers and induce a redistribution of fibroblasts in the wound bed. A4) Image of the injured tissue: black arrows show tissue wounds.

Histology and immunohistochemistry

Skin samples were fixed in 10% formalin and then included in paraffin blocks: sections of 5 µm were obtained. Slides were stained with Hematoxylin and Eosin (H&E) (Histoline 01HEMH500) following internal procedures. For immune-labeling, three vertical tissue sections (from three independent experiments) were prepared from each histological slide. Immunofluorescence (IF) was performed to localize the following biomarkers: α-SMA and FN. The following primary monoclonal antibodies were used: α-SMA (Abcam, ref. ab7817, Mouse), FN (Sigma Aldrich, ref. ab2413, Rabbit). All secondary antibodies were diluted 1:400 in PBS 1x. DAPI was used for nuclei staining. The images were acquired with LEICA DMi8 THUNDER imager 3D System (Leica) (Leica sCMOS Camera and LASX 3.0.1 software).

Statistics

Statistical analyses on immunohistochemistry results were performed by an ANOVA-Tukey HSD test. The significance threshold was set for the Tukey HSD test as p-value < 0.01. For all data sets, experiments were repeated in biological triplicates in 3 independent studies.

Results

Keratinocytes nuclei orientation in Wound Model (WM)

Nuclei orientation in WM on day 3 is illustrated in Figure 2 by representative DAPI staining images. Nuclear shape and orientation in the wound on WM tissues (A_1) and unwounded tissue (NC) (A_2) are analyzed during the repairing process in the wound bed. FT-Skins were divided into three regions according to the wound gap position (wound bed, right edges and left edges) and orientation of the major axis of the nuclei of the basal cells in the epidermis was quantified.

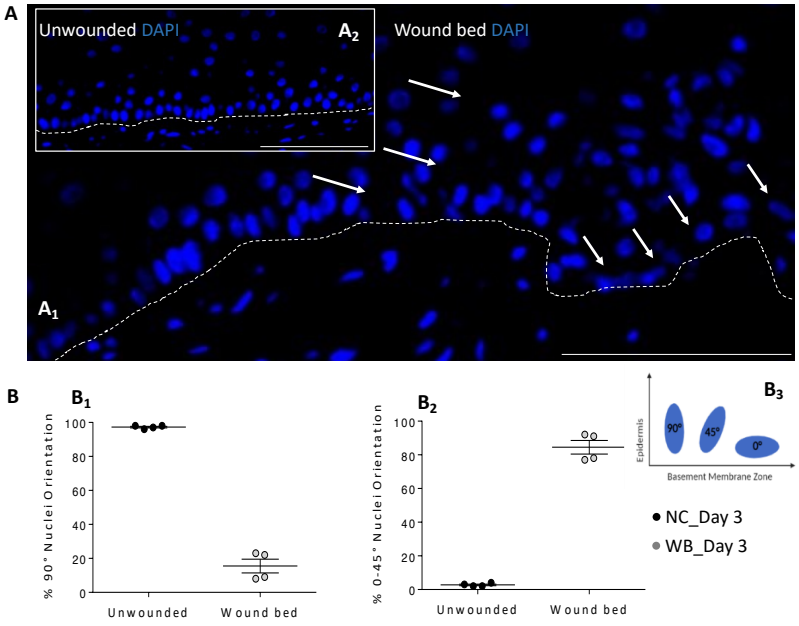

Figure 2. Nuclei orientation in the unwounded tissue (NC) and in the wound bed of WM. Data are generated from three independent experiments. A) Histological representation of nuclei stained with DAPI (blue) in wound bed (A_1) and in the NC (A_2) on day 3. White arrows indicate nuclei deformation. Dotted lines indicate dermal-epidermal junction. B) Nuclei orientation (90° and 0-45°) in NC and wound bed. Unwounded tissues show a distribution of nuclear orientations with a tendency towards 90° (B_1) while wounded tissues towards 0-45° (B_2). A Cartesian reference system was used where the X axis corresponds to the basal membrane (B_3). Magnification 40X. Scale bar: 100 mm. WM: wounded skin model, NC: negative control, WB: wound bed.

Dotted lines in panels A_1 and A_2 indicate dermal-epidermal junction while the white arrows indicate the nuclei shape modified in the wound bed of the skins. On day 3 from the injury, a distribution that significantly differed from rotation angles of nuclei in unwounded tissues has been observed in regions of wounded skin. In particular, nuclei-shape deformation increases moving from the unwounded lateral edges to the newly formed tissue. Nuclei orientation quantification is reported in Figure 2B revealing a preferential cell distribution (90% of total number of cells) in the wound bed of the WM compared to NC: unwounded tissues show a distribution of nuclear orientations with a tendency towards 90° (B_1) while wounded tissues towards 0-45° (B_2) when considering a Cartesian reference system where the X axis corresponds to the basal membrane (B_3).

Wound Model compared to Advanced Wound Model (WM vs AWM)

The repair dynamics was investigated in the WM and AWM by H&E staining (Figure 3 A-B) from day 1 to day 8. Figure 3A illustrates the morphological modifications related to re-epithelization process in the WM: epidermis seamlessly attached to the dermis compartment except in the wound area on day 1 (A_1), providing an *in vivo*–like matrix for re-epithelialization surrounded by clearly defined wound margins. Tissue continuity is destroyed in both epithelial and dermal compartment. The extending epidermal tongue is visible as 1-2 cell layers in the wound bed on day 3 (A_2): the presence of cells randomly distributed in the wound bed, corresponding to injury site, suggest formation of new tissue. The black arrow and the dotted line indicate the shift from the pre-existing tissue to a newly formed tissue. The keratinocytes covered 100% of the wound area on day 8 (panel A_3) by organizing the epithelium into approximately three cell layers near the wound edges and one cell layer in the center of the wound bed. The dotted line indicates the boundary between epithelium and dermis: keratinocytes are still visible in the wound bed.

Fig. 3B illustrates the re-epithelization in the AWM: as observed in the WM, epidermis seamlessly attached to the dermis compartment except in the wound area on day 1 (B_1) where modification occurred in both compartments. The edges of the wound appear slightly frayed, but gap appears smaller; probably, this is due to a greater tissue contraction. In panel B_2, keratinocytes have started migration and repair process and 100% of re-epithelialization is displayed in panel B_3 on day 8, where complete wound closure is reached. The tissue in the AWM wound bed appears less cellularized than the tissue in the WM. Despite this, total tissue repair has been observed both in the epidermis and in the dermis. The tissue morphology and wound dynamics are similar in both models (WM and AWM) but keratinocytes localization was shown to be different suggesting a greater involvement of ECM components in the AWM in surrounding the epithelial cells in the wound bed leading to a more efficient wound healing.

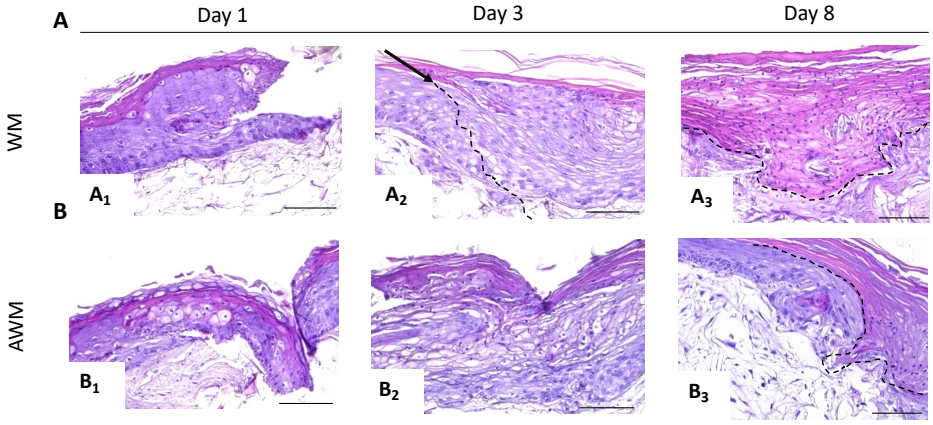

Figure 3. H&E on WM and AWM. Data are generated from three independent experiments. H&E stain shows morphological variation and progressive closure of wounds in WM and AWM on day 1 (A_1 - B_1), day 3 (A_2 – B_2) and day 8 (A_3 – B_3), respectively. The black arrow and the dotted line in A_2 indicate the shift from the pre-existing tissue to a newly formed tissue. The dotted line in A_3 and B_3 indicates the boundary between epithelium and dermis. Magnification 40X. Scale bar: 100 mm. H&E: WM: wounded skin model; AWM: advanced wound model.

Fibroblasts activation and newly ECM components in the wound bed

Fibroblast differentiation (cellular response) and newly ECM production were investigated on day 3 and day 8 in WM and AWM. Figure 4 shows the expression pattern by quantitative IF analyzes of α-SMA, marker of myofibroblast differentiation typical of fibroblast heterogeneity [9], and of FN, specific biomarker of granulation tissue.

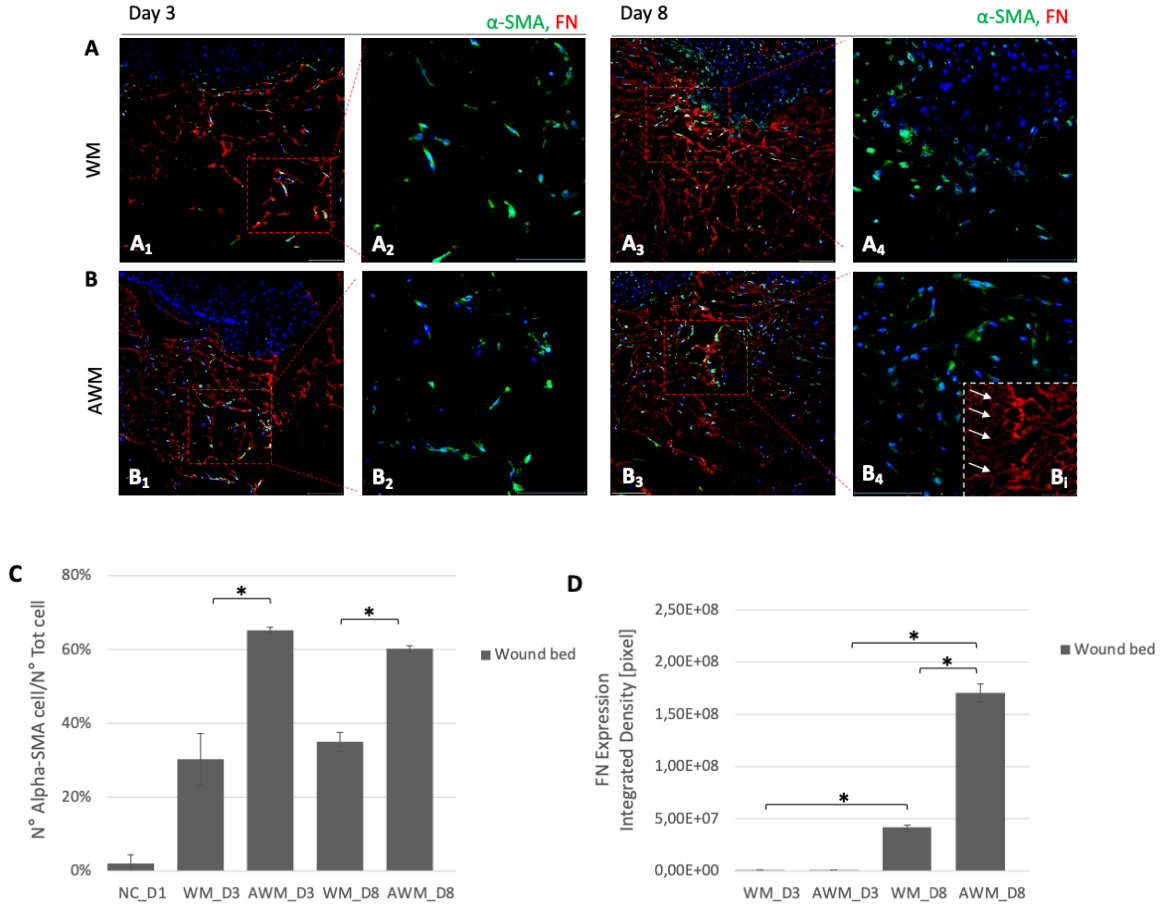

Figure 4 (A;B;C;D) : IF of a-SMA and FN on WM and AWM. Data are generated from three independent experiments; the figure includes representative fluorescent images of a-SMA (green) and FN (green) double staining in the newly formed tissue of the wounded bed in WM (A) and AWM (B) on day 3 (A_1 - B_1) and day 8 (A_3 - B_3), respectively. The red squares in panel A_1 and A_3 highlight fibroblasts activation in the dermis wound bed as visible in A_2 and A_4 for a-SMA in WM on day 3 and day 8, respectively. The red squares in panel B_1 and B_3 highlight fibroblasts activation in the dermis wound bed as visible in B_2 and B_4 for a-SMA in AWM on day 3 and day 8, respectively and in B_i for FN in AWM on day 8. C) Quantitative analysis of the number of a-SMA-positive cells with respect to the total nuclei number in wound bed and edges on day 3 and day 8. NC (FT-Skin non-injured and non-treated) on day 1 is used as tissue control. D) Quantitative analysis of FN expression in pixel calculated as integrated density area in wound bed and edges on day 3 and day 8. Nuclei are stained with DAPI (blue). Magnification 20X and 40X. Scale bar: 100 mm. Statistical significance between samples is reported as *($p<0.01$) according to ANOVA-Tukey HSD test. FN: fibronectin; NC: negative control; WM: wounded skin model; AWM: advanced wound model.

In Fig. 4A the results obtained in the WM on day 3 and day 8 are shown: α-SMA-positive fibroblasts are randomly identified on day 3 (A_1-A_2), while only a signal featured by high background noise of FN was observed (A_1). On day 8 (A_3-A_4), α-SMA positive fibroblasts are mainly located around the tongue of the newly formed epidermis. Moreover, in the wound area, FN expression levels increase around α-SMA-positive cells (A_3): spotted signal of α-SMA positive fibroblasts corresponds to a strong red signal in the region of the wound.

In Fig. 4B the results obtained in the AWM on day 3 and day 8 are presented revealing a large ECM region in which fibroblasts are activated. ECM is populated by both cell populations in the wound bed and around the edges on day 3 (B_1-B_2). On day 8, the α-SMA signal increased and both cell populations are detected in the whole tissue (B_3-B_4). FN signal change overtime in the wound bed: a bright and pericellular signal was detected on day 3 while a strong increased FN signal is detected on day 8 (B_3). Red and green signals co-localization are detected on day 8 (B_3-B_4) indicating correlation between fibroblasts activation and FN production/expression at this timepoint. The insert B_i marks this correlation showing the strong red signal in the center of the wound bed highlighting the huge amount of FN after the tissue has been repaired. In Fig. 4C quantification of cell density and the regulation of α-SMA expression levels in WM is reported. Analyses was performed in the wound bed of both WM and AWM confirming the almost absence of positive α-SMA fibroblasts in negative non injured control. The expression levels of α-SMA in WM are 30 and 35 times higher than control (NC) on day 3 and day 8, respectively ($p < 0.01$). The expression levels of α-SMA in AWM are 65 and 60 times higher than control (NC) on day 3 and day 8, respectively ($p < 0.01$). These data confirm fibroblasts response and activation to both injury and treatment with L-AA. They also support a statistical difference between WM and AWM both at day 3 and day 8 ($p < 0.001$). Indeed, α-SMA positive fibroblast population is predominant in AWM compared to WM. In WM the a-SMA positive fibroblast population corresponds to the 30% and 35% of the whole cell population, while in AWM it corresponds to the 65% and 60% on day 3 and day 8, respectively. Globally, α-SMA expression is increased in the whole tissue of the AWM: 50% of fibroblasts are α-SMA-positive after 8 days of culture with surplus of L-AA. Fig. 4D reports quantitative analysis of FN expression in WM and AWM on day 3 and day 8. The data suggest that no statistical difference in the amount of FN is found between WM and AWM on day 3 and IF signals are almost absent in the wound bed in both models. On the contrary, FN expression levels increase significantly on day 8 for both models. Statistical difference obtained from day 3 to day 8 ($p < 0.01$) highlights a time-dependent ECM production. The expression level of FN in AWM is 4 times higher than WM on day 8 ($p < 0.01$). These results are useful to demonstrate the robustness of the AWM and they confirm the role of L-AA in supporting FN production.

Discussion

The remodeling process in the 2 series (WM and AWM) are similar but the connective tissue repairs and reorganizes itself in a completely different structure. While in the WM fibroblasts are the main population of the dermis except in the wound gap, in the AWM two cell populations have been identified: fibroblasts and myofibroblasts. Furthermore, the high number of myofibroblasts in tissue areas in the AWM is consistent with high FN expression level. This observation agrees with a study conducted by Lombardi et al., which also showed the appearance of cell differentiation and increase in the levels of FN in an organotypic wounded dermal model [10]. The morphology and feature of AWM confirm the role of L-AA in ECM deposition/remodeling resulting in dermis architecture reinforcement and an increase of dermal response to injury.The AWM allows to investigate the cellular machinery and dynamics involved in the full ECM repair process in a relative short experimental window.

Conclusion

The experimental model developed on FT-skin recapitulates in a reduced time course the main steps of skin regeneration process and it is a promising candidate as robust, reproducible and relevant preclinical model to investigate the skin regeneration properties of topically or systemically applied ingredients. In addition, it could provide a good experimental system to address myofibroblasts, which are confirmed as main actors in tissue granulation and wound contraction and as key target to counteract insufficient skin repair and/or excessive fibrosis. Being AWM more performant and responsive than WM, it may be applied in testing novel antiscar strategies by monitoring FN expression.

Conflict of Interest Statement.

The authors have no conflict of interest to declare

References.

1. Ling TZ, Nather A, and Dennis HHW (2012) Basic science of wound healing, Diabet. Foot 89–96.
2. Desjardins-Park HE, Foster DS, and Longaker MT (2018) Fibroblasts and wound healing: An update Regen. Med. 13(5):491–495.
3. Volk SW, Wang Y, Mauldin EA, Liechty KW, and Adams SL (2001) Diminished type III collagen promotes myofibroblast differentiation and increases scar deposition in cutaneous wound healing Cells Tissues Organs 194(1):25–37.
4. Tomasek JJ, Gabbiani G, Hinz B, Chaponnier C, and Brown RA (2002) Myofibroblasts and mechano-regulation of connective tissue remodelling Nat. Rev. Mol. Cell Biol. 3(5):349–63.
5. Darby IA, Laverdet B, Bonté F, and Desmoulière A (2014) Fibroblasts and myofibroblasts in wound healing Clin. Cosmet. Investig. Dermatol. 4(7):301–311.
6. Ackermann K, Lombardi Borgia S, Korting HC, Mewes KR, and Schäfer-Korting M (2010) The phenion® full-thickness skin model for percutaneous absorption testing Skin Pharmacol. Physiol. 23(2):105–112.
7. Mewes KR, Raus M, Bernd A, Zöller NN, Sättler A, and Graf R (2007) Elastin expression in a newly developed full-thickness skin equivalent Skin Pharmacol. Physiol. 20(2):85–95.
8. Zöller NN, Kippenberger S, Thaçi D, Mewes K, Spiegel M, Sättler A, et al. (2008) Evaluation of beneficial and adverse effects of glucocorticoids on a newly developed full-thickness skin model Toxicol. Vitr. 22(3):747–759.
9. Hinz B, Celetta G, Tomasek JJ, Gabbiani G, and Chaponnier C (2001) Alpha-smooth muscle actin expression upregulates fibroblast contractile activity Mol. Biol. Cell 12(9):2730–2741.
10. Lombardi B, Casale C, Imparato G, Urciuolo F, and Netti PA (2017) Spatiotemporal Evolution of the Wound Repairing Process in a 3D Human Dermis Equivalent Adv. Healthc. Mater. 6(13):1–11.